TECHNICAL MEMORANDUMS

NATIONAL ADVISORY COMMITTEE FOR AERONAUTICS

No. 632

DOWNWASH MEASUREMENTS BEHIND WINGS WITH DETACHED FLOW

By E. Petersohn

Zeitschrift für Flugtechnik und Motorluftschiffahrt
Vol. 10, No. 22, May 28, 1931
Verlag von R. Oldenbourg, München und Berlin

Washington
August, 1931

NATIONAL ADVISORY COMMITTEE FOR AERONAUTICS

TECHNICAL MEMORANDUM NO. 632

DOWNWASH MEASUREMENTS BEHIND WINGS WITH DETACHED FLOW*

By E. Petersohn

In ordinary airplane-stability calculations which are applicable only to normal flight (i.e., with contiguous flow), it generally suffices to know only the direction of the downwash, while the velocity variations behind the wing are of subordinate importance. With a detached or separated flow, however, these velocity variations are very great and of considerable importance in the determination of the stability. In order to obtain data on this problem, an investigation of the velocity conditions behind wings has been made by the Göttingen Aerodynamic Institute.

The investigation, which was made in the small wind tunnel having a diameter of 1.2 m (3.94 ft.), embraced three wing models, behind which, at various angles of attack between 0 and 60°, the static pressure and the total pressure along various vertical lines (perpendicular to the direction of the undisturbed wind and to the wing span) were measured. The locations of these vertical lines are indicated in Figure 1. Moreover, the wing polars were determined by the customary three-component measurements.

For testing the pressure field, a Pitot tube and a static probe, both of 2 mm (0.08 in.) diameter, were mounted 40 mm (1.57 in.) apart on the end of a shaft 1 m (39.37 in.) long, as shown in Figure 2. The shaft was attached to a support outside the air stream in such a way as to afford the three following possibilities of motion: a, motion in the direction of its length; b, vertical motion parallel with itself; c, rotary motion about the axis AB. (Fig. 2.) The latter was necessary for adjusting the tube in the direction of the wind. The pipes from the static probe and Pitot tube led through the shaft to the manometer. The static pressure was measured by an oblique Recknagel tubular manometer, while the total pres-

*"Abwindmessungen hinter Tragflügeln mit abgerissener Strömung." From Zeitschrift für Flugtechnik und Motorluftschiffahrt, May 28, 1931, pp. 289-300, published by R. Oldenbourg, Munich and Berlin.

sure was measured by a vertical Prandtl tubular manometer. The whole test set-up is shown in Figure 3. Since the flow near the plane of symmetry of the wing may be regarded as nearly two-dimensional, the measurements in this plane were made with the Pitot tube and the static probe placed symmetrically with respect to it. In making the measurements at the lateral points, the shaft was so shifted between the readings of the two pressures, as to bring the proper instrument to the desired point.

The three following wings were investigated, all having the Göttingen 387 profile (fig. 1):

1. Rectangular wing 130 × 520 mm (5.12 × 20.47 in.), aspect ratio 4;

2. Rectangular wing 92 × 736 mm (3.622 × 28.976 in.), aspect ratio 8;

3. Tapered wing, as in Figure 1.

For wings 1 and 2, the wind velocity was about 33 m/s (108.3 ft./sec.). For wing 3, it was about 28 m/s (92 ft./sec.). Since it has been found that, for tapered wings, the Reynolds Number, which diminishes toward the wing tips, has a certain influence in model tests, a wire screen of 1 mm (0.04 in.) wire and 8 mm (0.315 in.) was placed in front of the wing, in order to avoid this influence as much as possible by producing artificial turbulence.

The test results showed very little scattering and could be easily connected by a curve. (Fig. 5.) The symbols used in representing the test results are defined in Figure 4. In Figures 6-11, the test points are omitted for the sake of clearness. All pressures are divided by the dynamic pressure $q_o = \frac{\rho}{2} v^2$ of the undisturbed flow. Hence the plotted values represent nondimensional proportionality factors. The plain lines show the course of the total pressures p_g/q_o, while the dash lines represent the static pressures p/q_o. The static pressure in the undisturbed flow is taken as the zero point of the pressures. The vertical ordinates z/t represent the position of the test points and their height above the leading edge of the wing. In Figures 6, 8 and 10 the zero lines of pressure are so located that they simultaneously indicate the location of the test points with respect to the wing.

The tapered wing shows an increase in the total pressure on both sides of the blanketed area up to about 8% as compared with the undisturbed flow. (Fig. 15.) Comparative tests, without the turbulence screen, showed that this pressure increase was due to the screen. This phenomenon is explained by the fact that the flow velocity is reduced by the screen, so that the loss of energy from the screen in the middle of the air stream, where the wing hangs, is smaller than in the less disturbed portions of the stream. This was therefore corrected by referring the pressures measured in the blanketed area to a dynamic pressure corresponding to a maximum total pressure of $p_{g_{max}}$, instead of to the pressure p_{g_o} measured in the undisturbed flow. The corrected values are plotted in Figures 10 and 11.

In the three-component test the already known phenomenon was observed that, within a certain angle-of-attack range (about 15 to 35°), different flow conditions obtain, according to whether the wing is first adjusted and then subjected to the air blast, or whether the wing is adjusted in the wind and then reduced from larger angles of attack to the one at which the test is made, or whether the wing is adjusted in the wind and then raised from smaller angles of attack to the one at which the test is made. The first two cases generally yield the same flow. It may happen, however, that all three cases yield different kinds of flow. The first case then yields a lift between those measured in the last two cases. In the experiments reported here, the wing was always adjusted before the wind was turned on. The polars are represented by the plain lines in Figures 12 to 14.

With the exception of the static-pressure curves shortly behind the wing, the pressure-distribution curves show unexpectedly great symmetry at small angles of attack. The dissymmetry of the static pressure near the wing is explained by the fact that the circulation about the wing is here very noticeable.

Another phenomenon, which is of more theoretical than practical interest, is evidenced by the two static-pressure minima in the vicinity of the wing at large angles of attack in the transition zone between "dead water" and the undisturbed flow. These are probably due to the "Karman vortices" developed here.

At a few points the measured total pressure falls below the static pressure. In the cases where this happens, there is a reversed flow, so that the tubes are blown on from the rear. Here the instruments indicate a negative pressure.

Moreover, in the case of detached flow, there is a great negative pressure immediately behind the wing. This can probably be explained as follows. When the flow is detached, the lift distribution assumes the form shown in Figure 16a. The distribution of the vortices according to the known rules of the wing theory, will accordingly take the form shown in Figure 16b, that is, there are developed, in the vicinity of the middle of the wing, quite strong vortices, which produce the great negative pressure. In agreement with this explanation, as shown in Figure 26, is the phenomenon that, near the wing, where the vortices are not yet piled on one another, the negative pressure, with increasing angle of attack, reaches its maximum shortly after the separation. The reduction of the negative pressure at still greater angles of attack is due to the fact that, with increasing angle of attack, both the lift maxima travel toward the wing tips, whereby the vortices passing off from the middle of the wing gradually spread toward the wing tips.

Figures 7, 9 and 11 show how the magnitude of the blanketed area decreases toward the wing tips. This reduction is due to the fact that the effective angle of attack grows smaller toward the wing tips. This is particularly noticeable at small angles of attack. With the tapered wing (fig. 11) this reduction is increased by the diminishing wing chord.

For aviation purposes it is clearer to represent the results on a system of coordinates fixed with respect to the airplane. In Figures 17 to 19 the limits of the blanketed areas (i.e., the areas where there is a reduction in the total pressure) in the plane of symmetry are plotted for the different wings and angles of attack. It follows that, after the complete separation of the flow, the form of the blanketed area is nearly independent of the shape of the wing. This is decisive only for the angle at which the separation begins.

Pressure-distribution curves for a few lines perpendicular to the wing chord in the plane of symmetry were

determined from the measured pressure-distribution curves in Figures 20 to 22. These lines serve as the zero lines for the corresponding pressures. From these curves it is very easy to determine to what force variations any control surface behind the wing is exposed at different angles of attack. Of especial interest are the maximum pressure variations indicated by the enveloping curves of the various groups of curves. In Figures 23 and 24 these enveloping curves are reduced to one and the same chord for the investigated wing. The curves for the different wings are quite similar. It follows that the angle of attack, at which separation occurs, has little effect on the shape of the enveloping curves. This is probably due to the fact that, in the transition zone from the contiguous to the detached flow, a smaller blanketed area is connected with a greater deflection.

In order to present the results in a clearer manner, several groupings are made in Figures 26 to 31. In Figure 26 the maximum total pressure variations $\bar{p}_g/q_o$ in the plane of symmetry of the wing are plotted against the angle of attack. The parameter is x/t, in which x is the distance of the given section, perpendicular to the undisturbed flow, from the leading edge of the wing, and t is the wing chord. It is clearly seen how rapidly the pressure decreases on separation. In a similar way Figure 27 represents the integral of the total pressure change g in the plane of symmetry of the wing, after being made nondimensional by dividing by the dynamic pressure and the wing chord. This integral is very closely connected with the profile drag of the wing.

Figure 28 represents the deflection f of the blanketed area, f being measured perpendicularly to the direction of the undisturbed wind from the center of the chord to the center of the blanketed area. The center of the chord is determined as shown in Figure 25. In the detached flow the deflection is very small, due to the vortices passing off from the middle of the wing, which oppose the end vortices.

Figures 29-31 show, for a given section, the distribution of $\bar{p}_{g_1} q_o$ and f along the wing span. The x/t values are so chosen that the corresponding $x/\sqrt{F}$ values (F = wing area) for all three wings are the same.

In order to enable the calculation of the maximum

variations in the total pressure for other cases, an attempt was made to develop an empirical formula on the basis of the results obtained. The measured variations in the total pressure were therefore plotted against a reduced distance of $\bar{x} = \frac{x}{t \sin \alpha}$ behind the wing. (Fig. 32.) It was found that, for a completely detached flow, the points obtained for the various angles of attack lie on one and the same curve. For $\bar{x}$ values greater than 3 to 5 this curve can be represented by the equation

$$\frac{\bar{p}_g}{q_o} = \frac{5}{\bar{x}}\left(1 + \frac{a}{\bar{x}}\right)$$

in which a is a constant depending on the wing contour. For the rectangular wing with an aspect ratio of 4, $a = 0.8$. For the rectangular wing with an aspect ratio of 8, $a = 2.4$. For the tapered wing, $a = 0$. These seemingly great variations in the the value of a have but little effect, however, on the value of $\bar{p}_g/q_o$.

A similar method with the dynamic-pressure values, however, yielded too great a scattering, so that it was not possible to connect the different points by a curve.

As already mentioned, all the measurements were made for one and the same wing profile. It is to be expected that the profile form will have but little effect when the flow is detached.

Summary

Behind a wing, after the separation of the flow, there is developed a very pronounced blanketed area, i.e., a diminution in the total and static pressures. The location of this blanketed area deviates but little from the direction of the undisturbed wind. The blanketed area seems to be nearly independent of the wing contour in both magnitude and direction.

Translation by Dwight M. Miner,
National Advisory Committee
for Aeronautics.

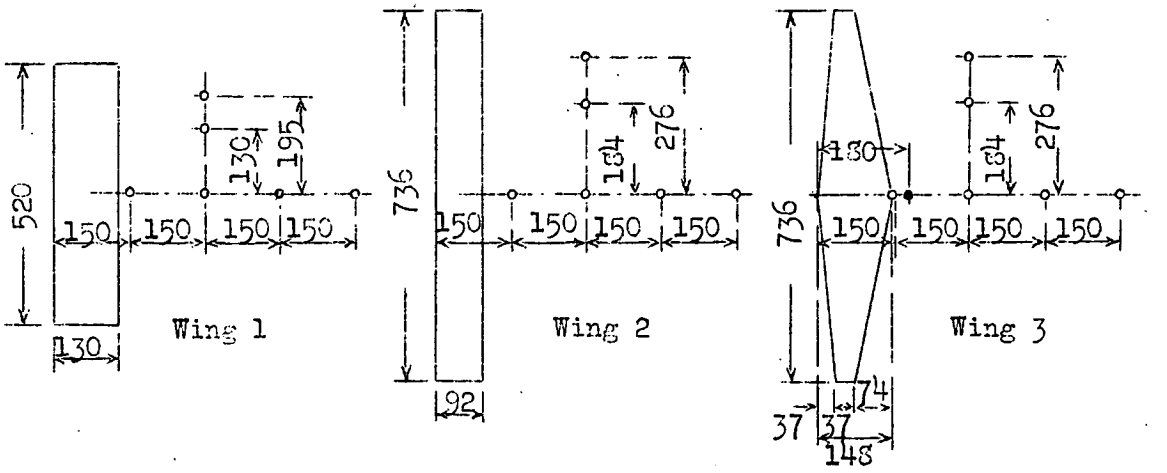

Fig.1, Dimensions of wing models and location of test points.

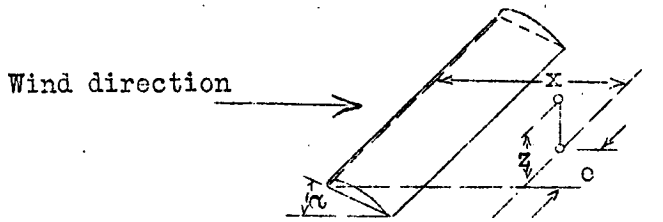

Fig. 4

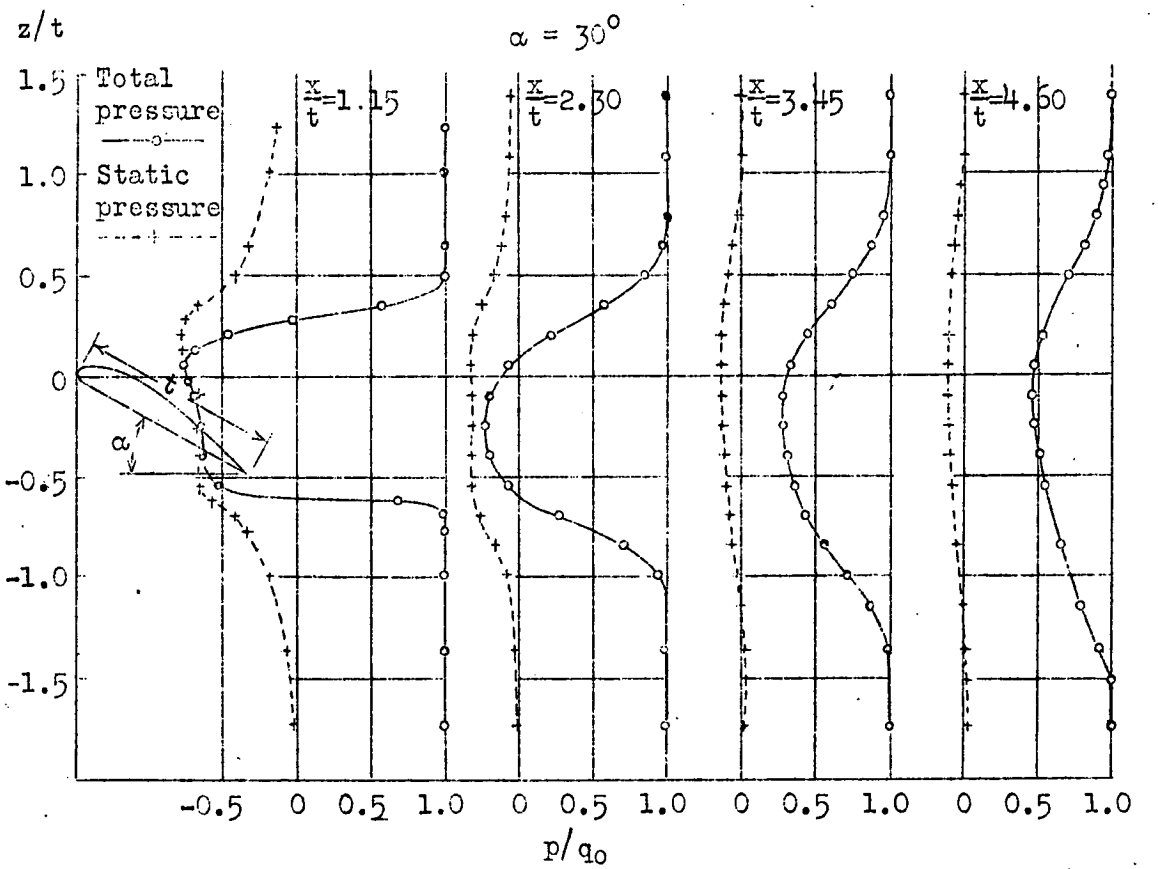

Fig.5, Example of test results. Rectangular wing. Aspect ratio 4

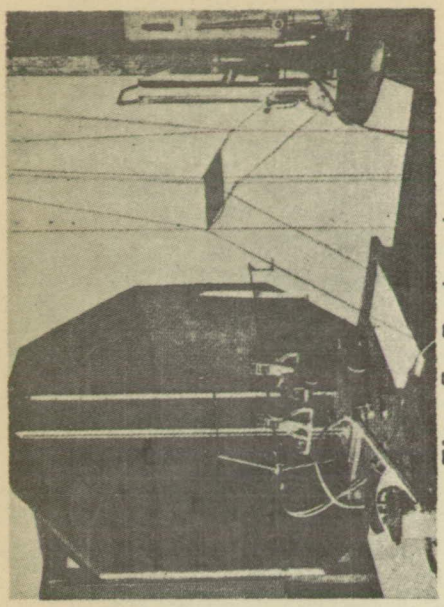

Fig. 3 Test set-up

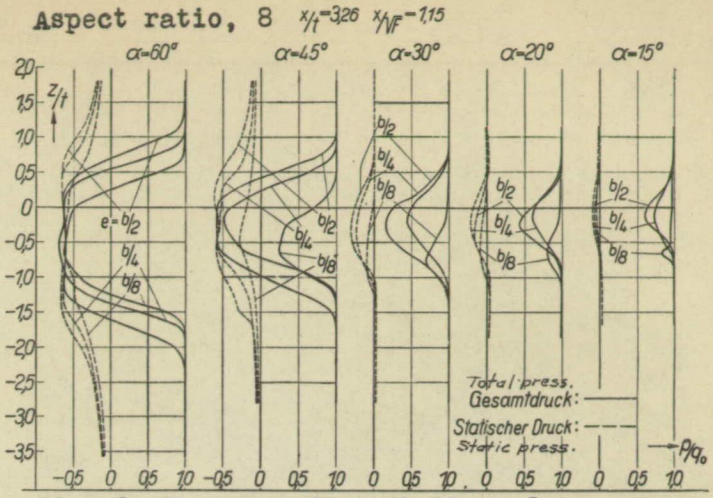

Fig. 9 Pressure distribution along span. Rectangular wing.

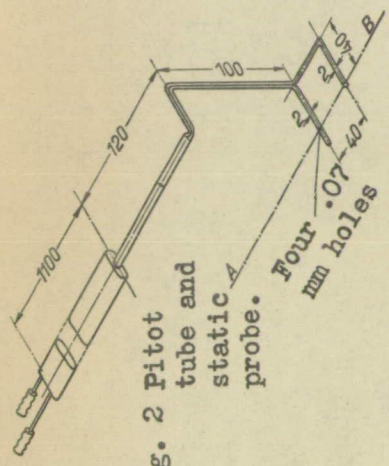

Fig. 2 Pitot tube and static probe.

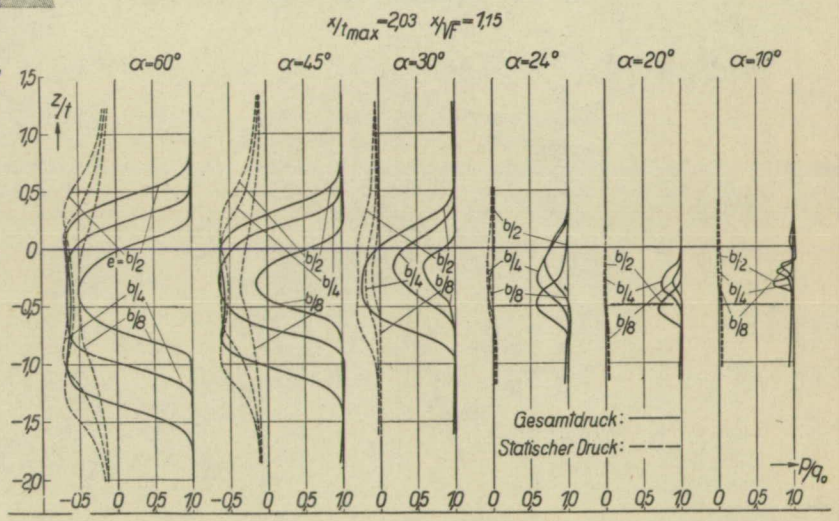

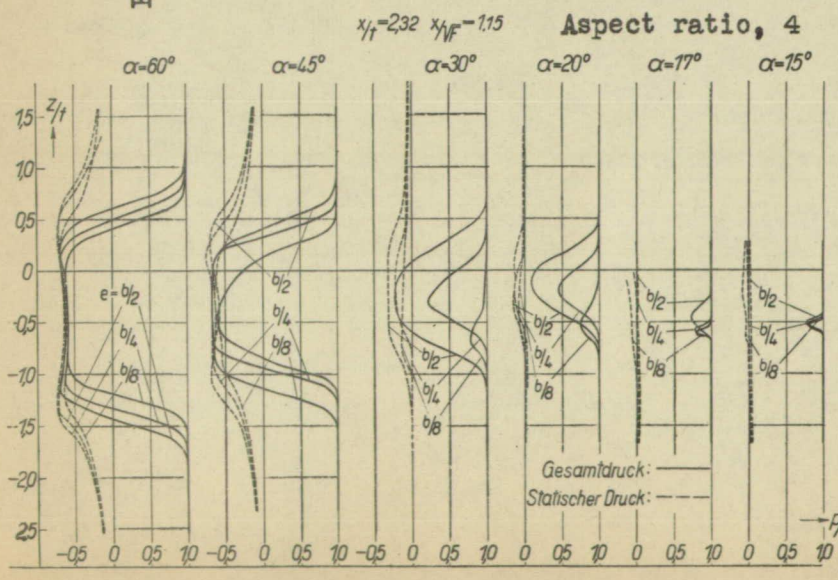

Fig. 11 Pressure distribution along span. Tapered wing.

Total pressure

Static pressure

Fig. 7 Pressure distribution along span. Rectangular wing.

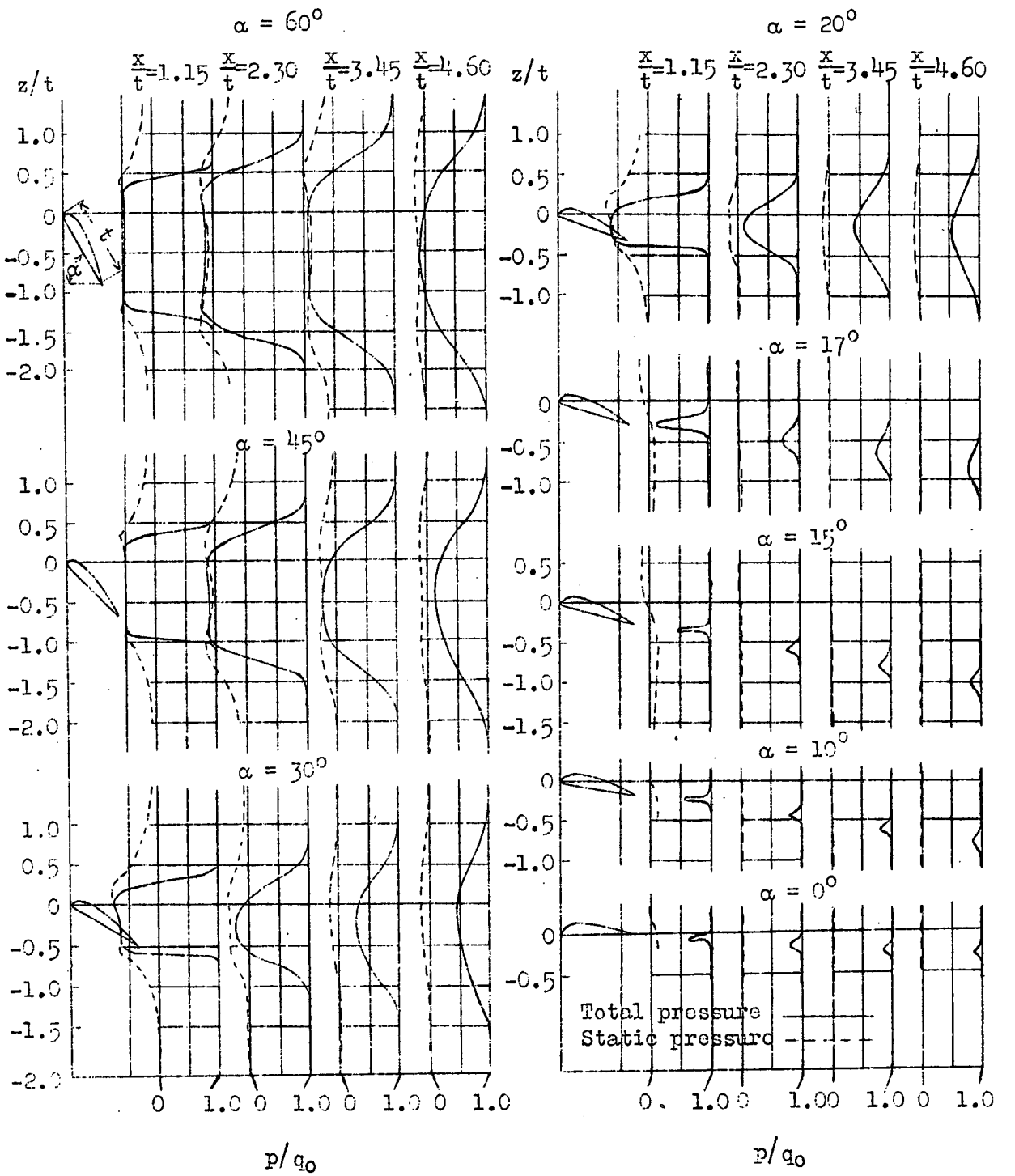

Fig. 6, Pressure distribution in plane of symmetry of wing. Rectangular wing. Aspect ratio 4

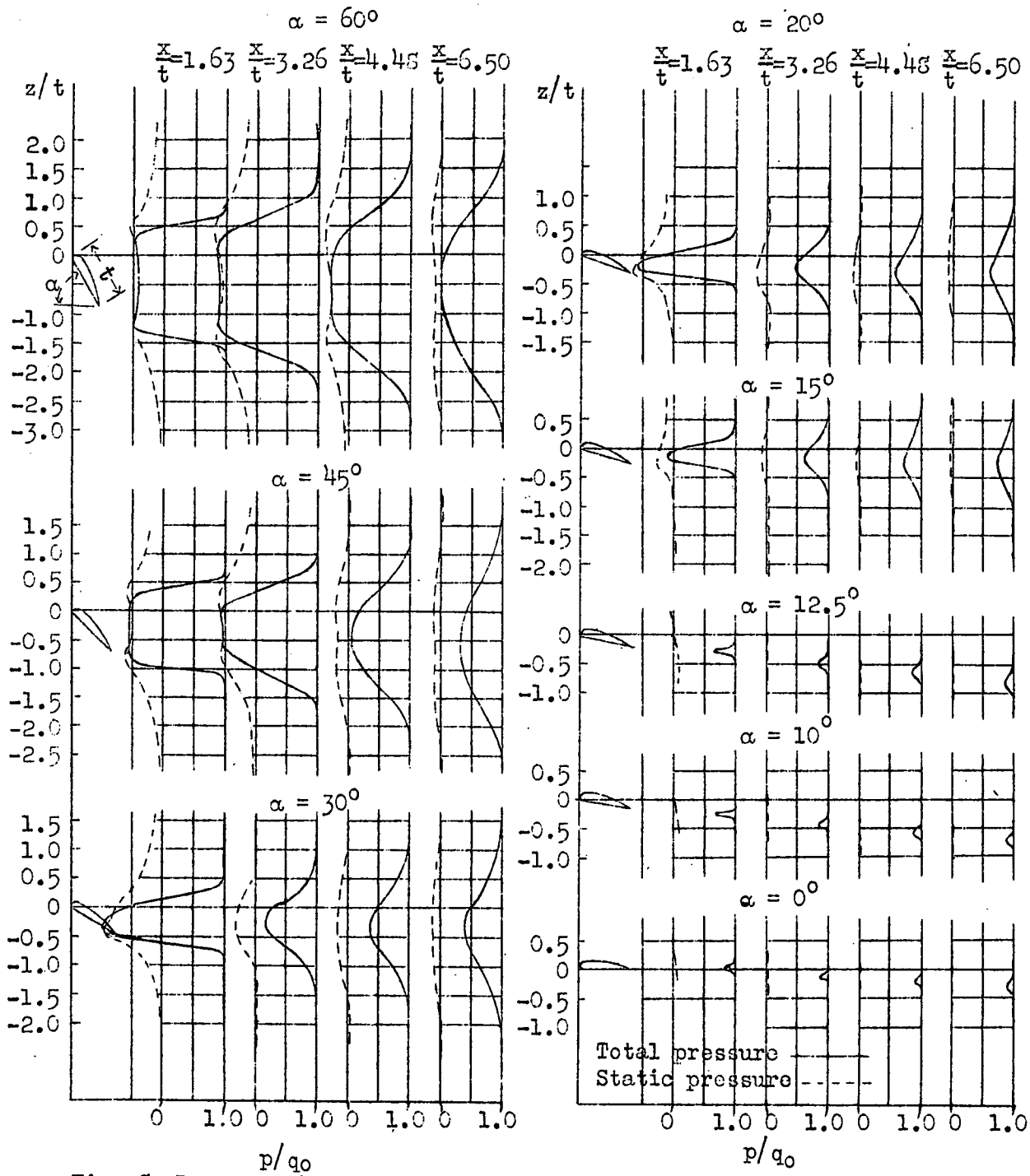

Fig. 8, Pressure distribution in plane of symmetry of wing. Rectangular wing. Aspect ratio 8

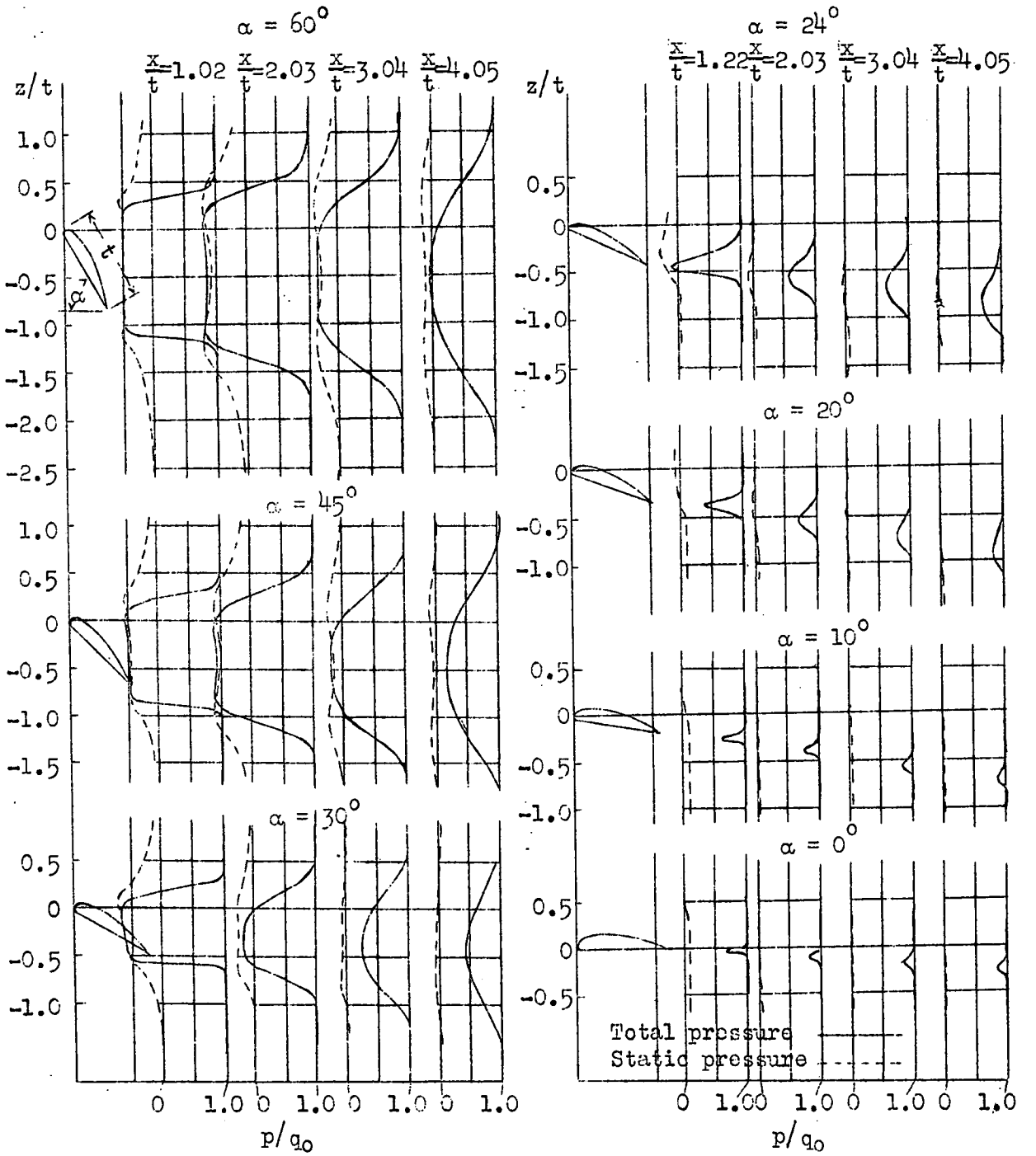

Fig.10, Pressure distribution in plane of symmetry of wing. Tapered wing.

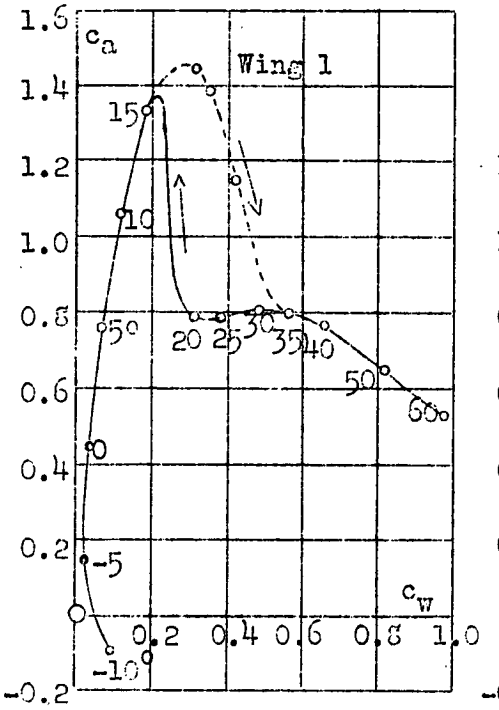

Fig. 12

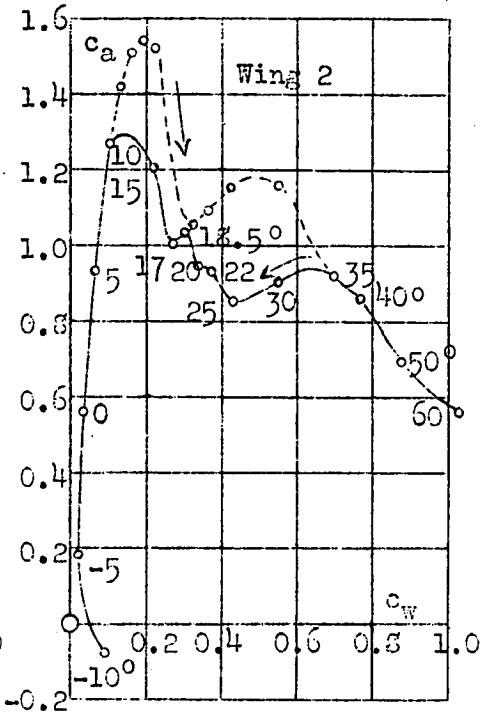

Fig. 13

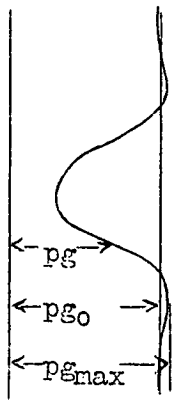

Fig.15, Effect of screen on pressure distribution behind wing in wind tunnel

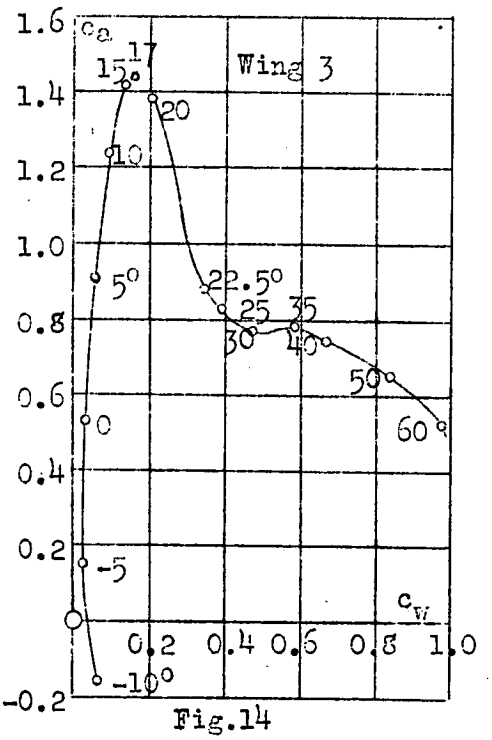

Fig.14

Figs.12.13.14, Polar curves of investigated wings

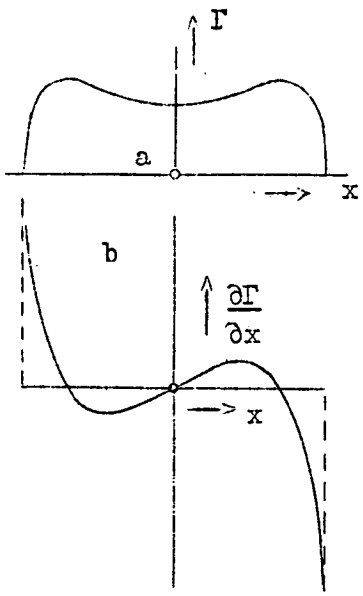

Fig.16, Lift and vortex distribution in detached flow

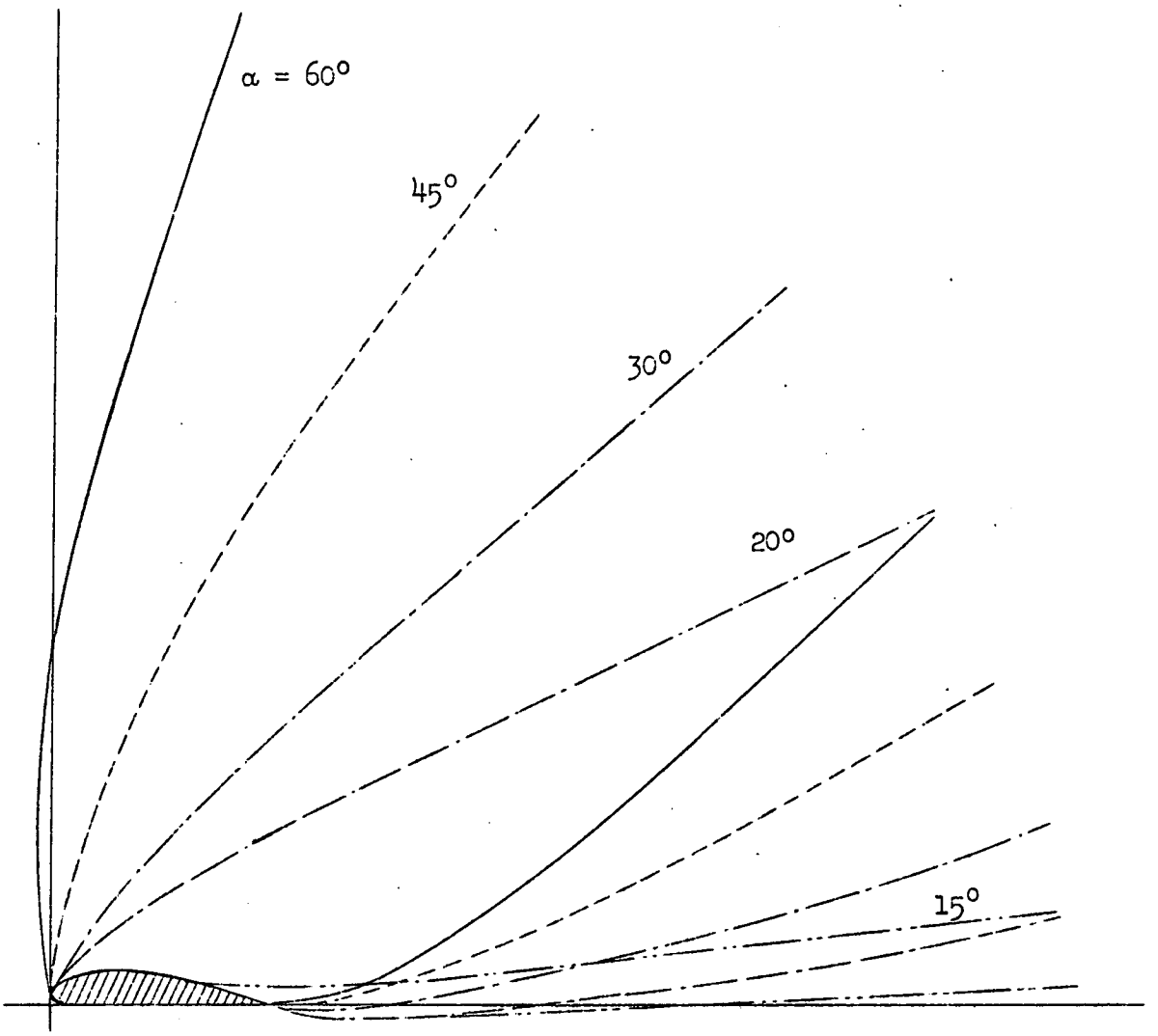

Fig.17, Limit of blanketed area with fixed wing and various angles of attack. Rectangular wing. Aspect ratio 4.

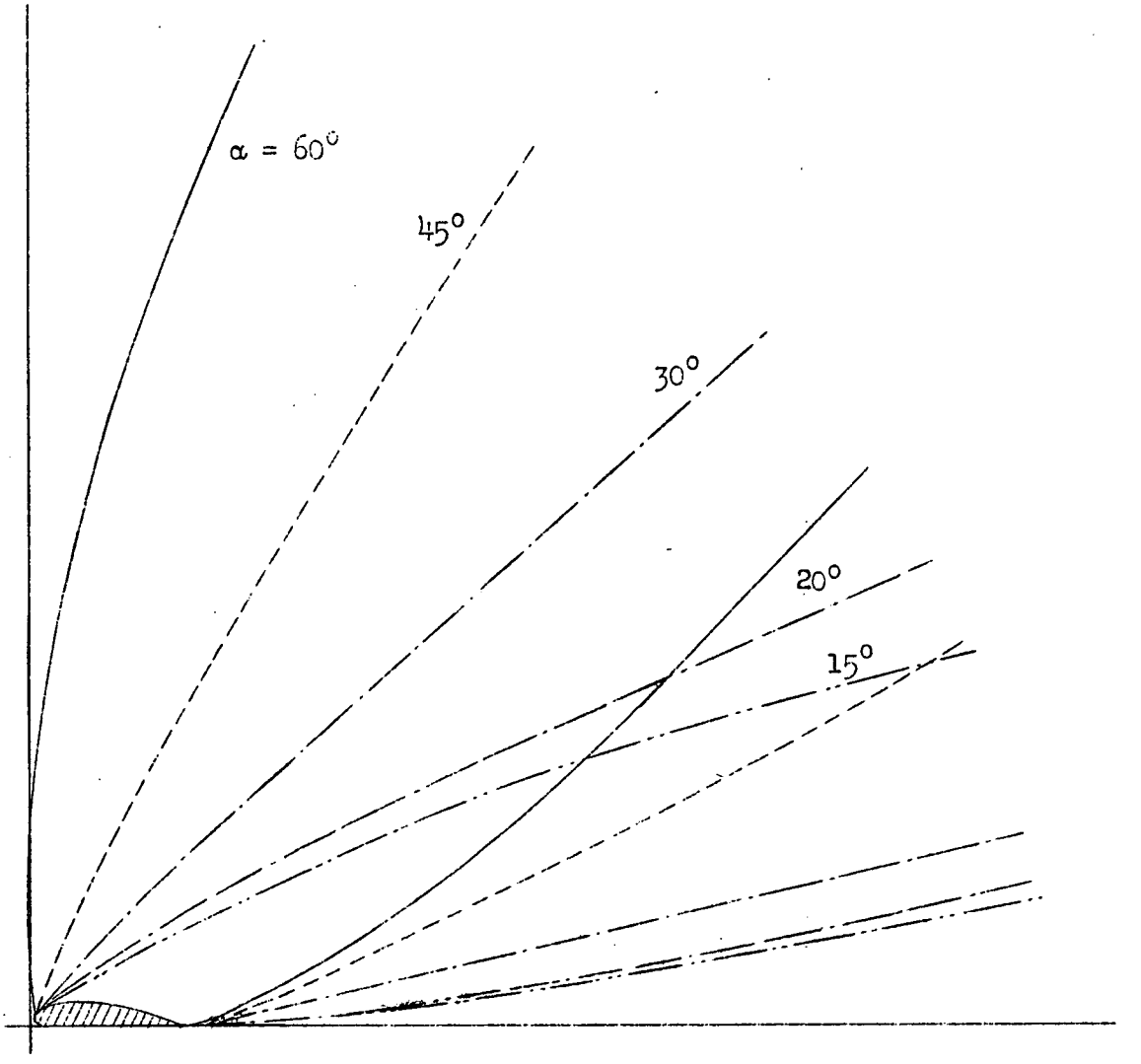

Fig. 18, Limit of blanketed area with fixed wing and various angles of attack. Rectangular wing. Aspect ratio 8.

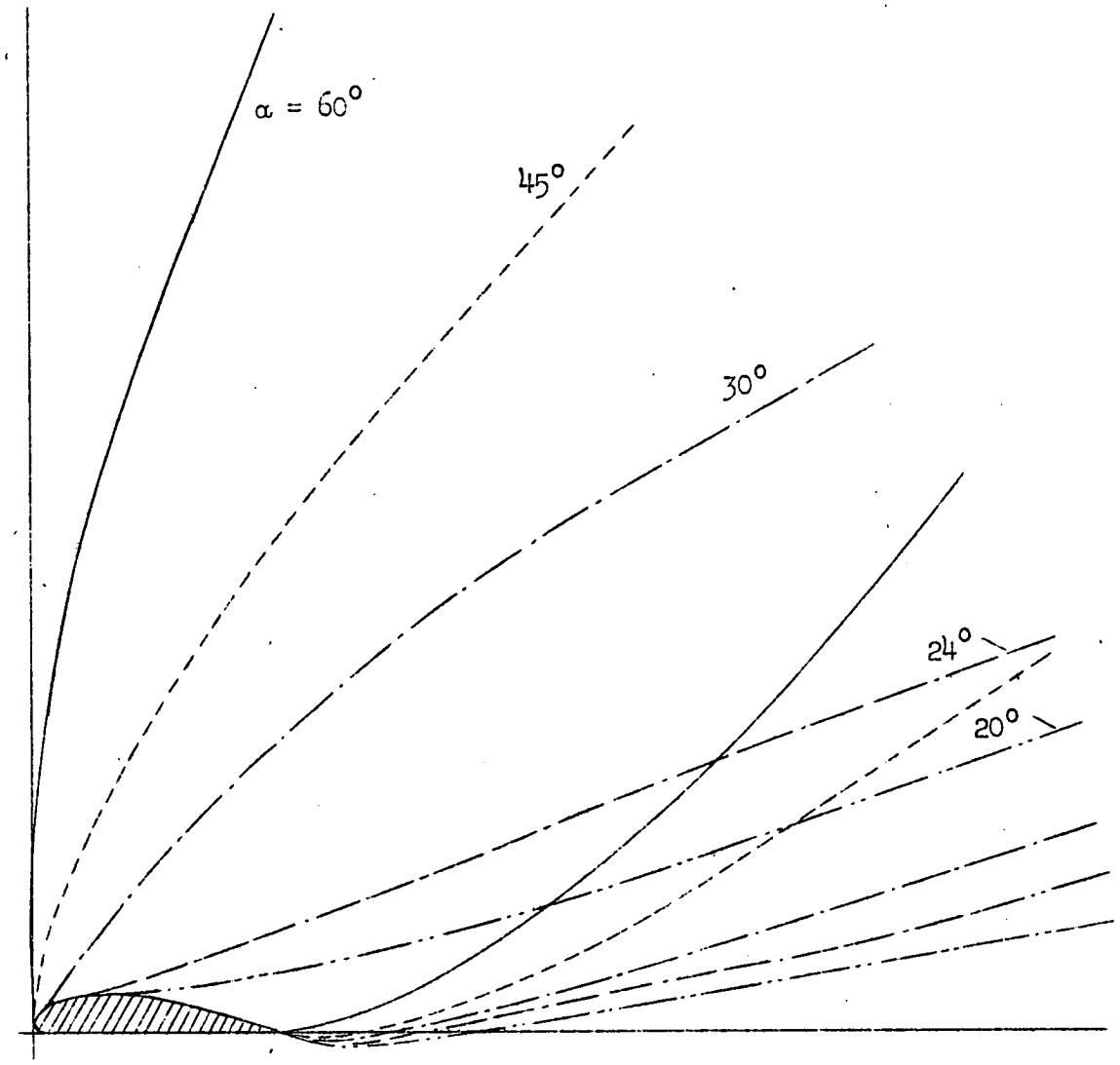

Fig. 19, Limit of blanketed area with fixed wing and various angles of attack. Tapered wing.

Figs. 20,21,22

Pressure distribution curves with fixed wing and different angles of attack.

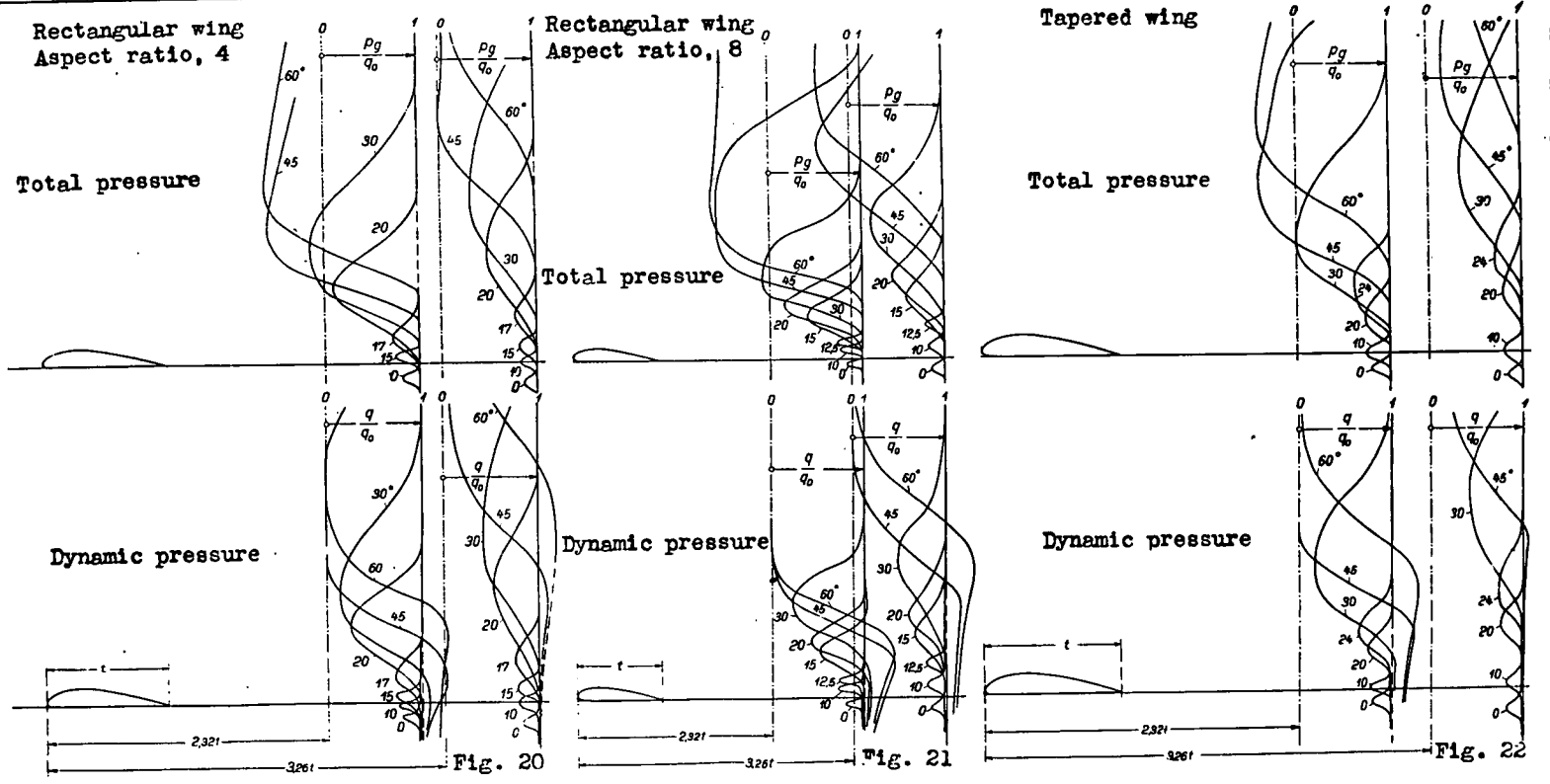

Fig. 20 Fig. 21 Fig. 22

Figs. 23,24

Enveloping curve of pressure distribution curves in Figs.20-22. Maximum pressure variation with fixed wing.

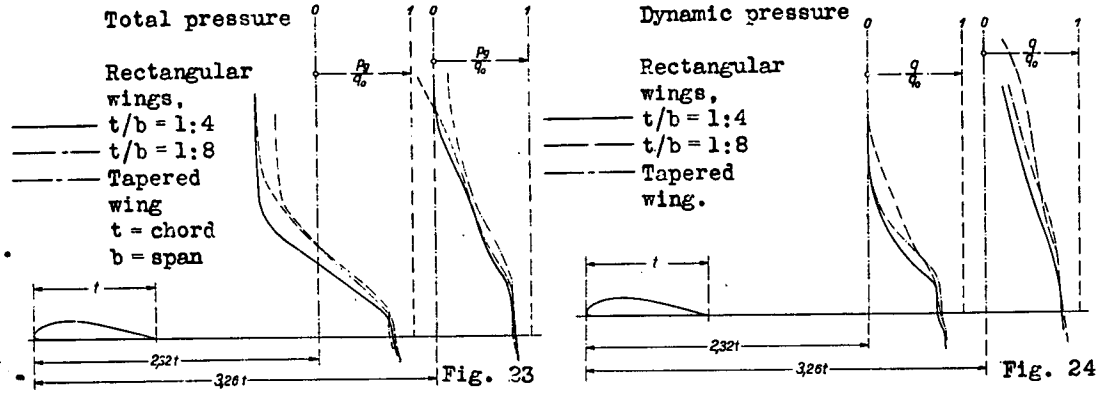

Fig. 23 Fig. 24

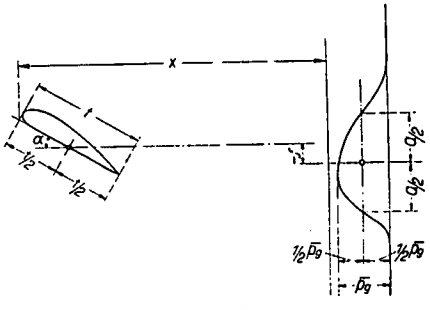

Fig. 25

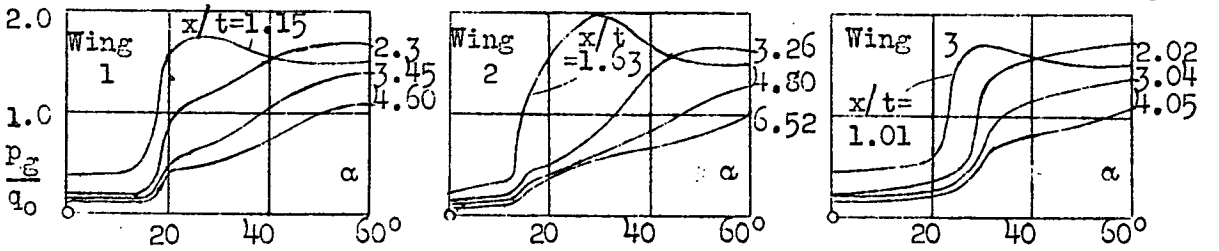

Fig.26, Maximum total-pressure variation $\bar{p}_g$ plotted against α

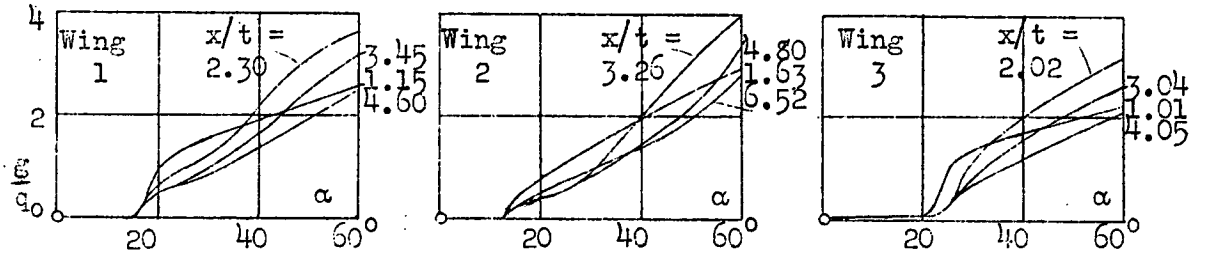

Fig.27, Integral of total-pressure variation g plotted against α

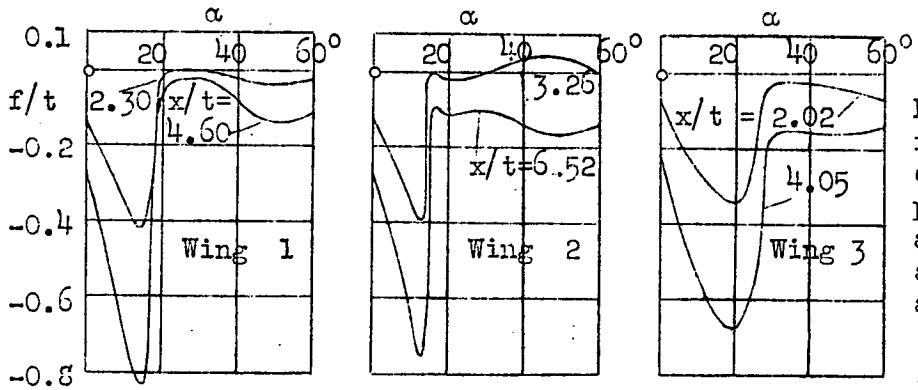

Fig.28 Deflection f of blanketed area plotted against angle of attack, α

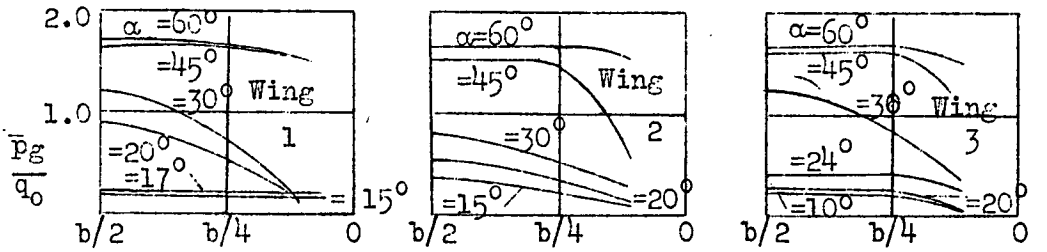

Fig.29, Maximum total-pressure variation along span.

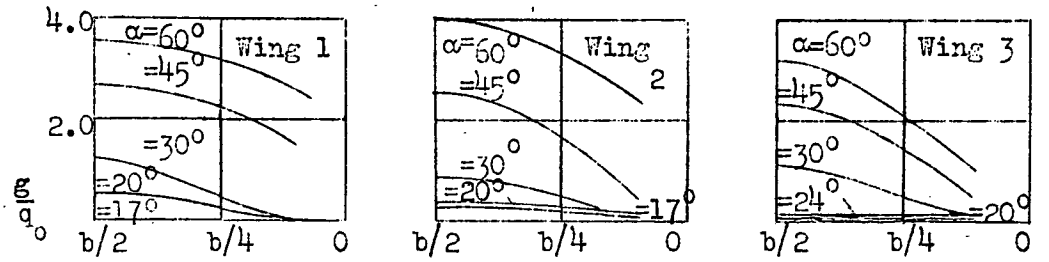

Fig.30, Integral of total-pressure variation along span.

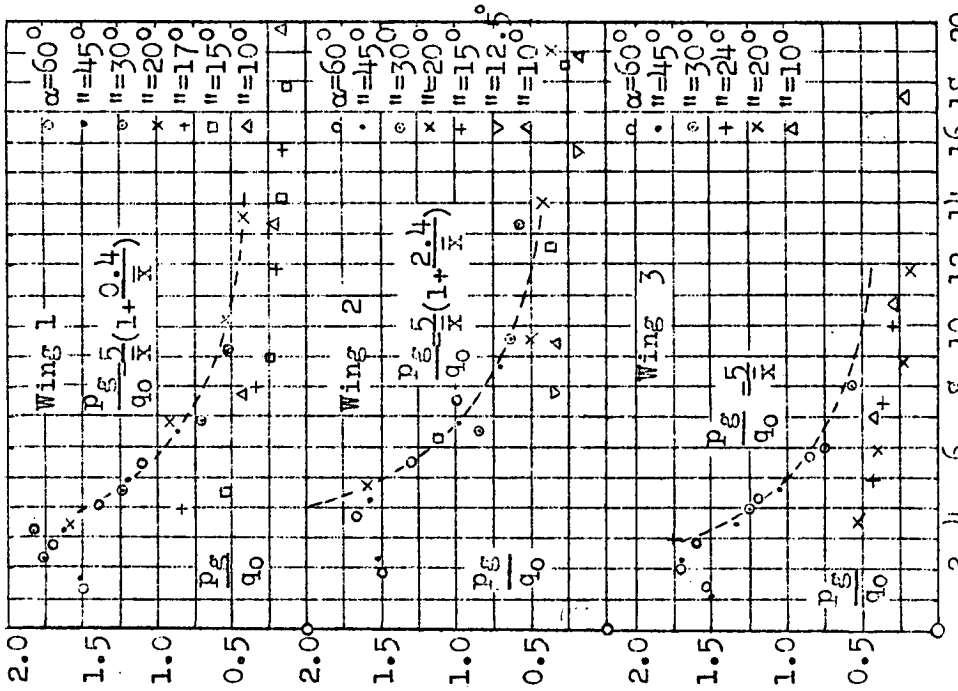

Fig.32, Maximum total-pressure variation p_g plotted against reduced distance $\bar{x} = \frac{x}{b \sin \alpha}$
Correction for wing 1,
$\frac{p_g}{q_0} = \frac{5}{\bar{x}}(1+\frac{0.8}{\bar{x}})$ instead of $\frac{pg}{q_0} = \frac{5}{\bar{x}}(1+\frac{0.4}{\bar{x}})$

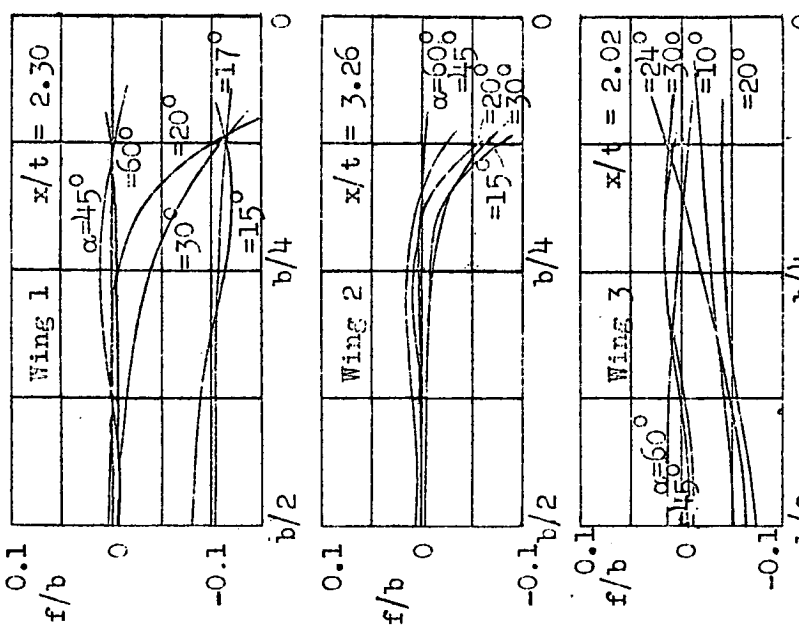

Fig.31, Deflection of blanketed area along span.